ARTICLE

Heterogeneous cancer-associated fibroblast population potentiates neuroendocrine differentiation and castrate resistance in a CD105-dependent manner

Manabu Kato[1] · Veronica R. Placencio-Hickok[2] · Anisha Madhav[2] · Subhash Haldar [2] · Manisha Tripathi[2] ·
Sandrine Billet[2] · Rajeev Mishra[2] · Bethany Smith[2] · Krizia Rohena-Rivera[2] · Priyanka Agarwal[2] · Frank Duong[2] ·
Bryan Angara[2] · David Hickok[2] · Zhenqiu Liu[2] · Neil A. Bhowmick[2]

Abstract

Heterogeneous prostatic carcinoma-associated fibroblasts (CAF) contribute to tumor progression and resistance to androgen signaling deprivation therapy (ADT). CAF subjected to extended passaging, compared to low passage CAF, were found to lose tumor expansion potential and heterogeneity. Cell surface endoglin (CD105), known to be expressed on proliferative endothelia and mesenchymal stem cells, was diminished in high passage CAF. RNA-sequencing revealed SFRP1 to be distinctly expressed by tumor-inductive CAF, which was further demonstrated to occur in a CD105-dependent manner. Moreover, ADT resulted in further expansion of the CD105$^+$ fibroblastic population and downstream SFRP1 in 3-dimensional cultures and patient-derived xenograft tissues. In patients, CD105$^+$ fibroblasts were found to circumscribe epithelia with neuroendocrine differentiation. CAF-derived SFRP1, driven by CD105 signaling, was necessary and sufficient to induce prostate cancer neuroendocrine differentiation in a paracrine manner. A partially humanized CD105 neutralizing antibody, TRC105, inhibited fibroblastic SFRP1 expression and epithelial neuroendocrine differentiation. In a novel synthetic lethality paradigm, we found that simultaneously targeting the epithelia and its microenvironment with ADT and TRC105, respectively, reduced castrate-resistant tumor progression, in a model where either ADT or TRC105 alone had little effect.

Introduction

Prostate cancer (PCa) is a heterogeneous disease that results in the second highest cancer mortality in men. The standard of care for recurrent PCa is the disruption of androgen signaling. The eventual development of resistance to androgen signaling deprivation therapy (ADT) has no curative approach. We had previously identified transforming growth factor-beta (TGF-β) signaling in fibroblasts as a determinant for prostate epithelial plasticity [1]. From the early steps of PCa initiation, the associated stromal fibroblastic cells begin to co-evolve with cancer progression and is predictive of recurrent disease and survival [2]. The tumor-inductive properties of cancer-associated fibroblasts (CAF) were originally coined as those that could convert non-tumorigenic epithelia to tumors and not simply based on proximity to cancer epithelia [3–5]. Additionally, prostatic CAF are attributed to tumor progression and therapeutic resistance to ADT [6, 7]. It is known that heterogeneous epithelial cell populations contribute to variable responses to treatments [8]. Whereas, the heterogeneity in the stromal fibroblastic cells is a concept less studied, especially in the context of resistance to therapy. Through a series of tissue recombination xenografts, we previously demonstrated the requirement of a heterogeneous mixture of mouse stromal fibroblasts with intact

These authors contributed equally: Manabu Kato, Veronica R.
Placencio-Hickok

✉ Neil A. Bhowmick
bhowmickn@cshs.org

[1] Nephro-Urologic Surgery and Andrology, Mie University
Hospital, Tsu, Mie, Japan

[2] Department of Medicine, Cedars-Sinai Medical Center,
Los Angeles, CA 90048, USA

and deficient TGF-β signaling to induce the initial transformation of benign epithelia into malignant lesions [9]. However, better understanding of the heterogeneous human prostatic fibroblast populations that support the expansion of established tumors and contribute to recurrent disease is needed.

Histologically similar fibroblastic cells that circumscribe the glandular epithelia of the prostate vary biologically. At a simplistic level, cell surface proteins can be used to differentiate fibroblastic cells much like distinct populations of histologically similar immune cells were distinguished over 30 years ago. Furthermore, the function of these surface proteins can be cell-type specific [10]. Mesenchymal stem cell proteins have emerged as markers for CAF in some tissues [11]. Among these markers, endoglin (CD105) was identified in both normal-associated fibroblasts (NAF) and CAF. Interestingly, extended culture of tumor-inductive CAF, can result in the loss of their inductive capacity through a change in fibroblastic heterogeneity [12]. We exploited the fact that culturing CAF can diminish its tumorigenic potential as a tool to explore the consequence of stromal heterogeneity and paracrine determinants of tumor progression. Fibroblastic population drift resulting from culturing primary fibroblasts was revealed to diminish the CD105 population and ensuing effects of tumorigenesis. CD105 is a TGF-β type III receptor that functions in promoting bone morphogenic protein (BMP) signaling and antagonizing TGF-β signaling. CD105 is found on proliferating endothelial cells in development and tumorigenesis [13]. We hypothesized that the CD105^{+} CAF population critically mediates prostatic tumor epithelial differentiation and castrate resistance in a paracrine manner.

Therapeutics for late stage PCa target the androgen axis by blocking androgen synthesis or the androgen receptor. The phase III PREVAIL trial demonstrated that enzalutamide, a direct androgen receptor inhibitor, improved overall survival by 2 months in castration-resistant prostate cancer (CRPC) patients who have not yet received chemotherapy [14]. Despite the initial efficacy of ADT many patients develop CRPC with the acquisition of neuroendocrine features by the cancer epithelia [15]. This paradox is a striking concept since de novo neuroendocrine PCa accounts for <1% of patients, yet 10–15% of patients develop tumors having neuroendocrine features following ADT as a treatment-emergent adaptive response [16]. The role of CAF on neuroendocrine differentiation has not been reported. Interestingly, multiple paracrine factors have been demonstrated to support resistance to ADT, including IL-6, Wnt ligands, and IGF-1 [6, 17, 18]. Here, we identify a stromal CD105-expressing population in CAF that can mediate neuroendocrine differentiation and CRPC in a paracrine fashion. We further show that CD105 is highly druggable and can serve as a target complementing ADT to restore castrate sensitivity.

Results

Stromal heterogeneity is observed in human PCa specimens

Prostatic fibroblast populations directly from prostatectomy tissues were studied to determine heterogeneity of associated fibroblasts. Once we characterized these tissues as cancer or benign with H&E staining, we dissociated and depleted them for EpCAM^{+} epithelia and CD45^{+} lymphocytes by magnetic separation. FACS analysis was performed to distinguish for previously established mesenchymal stem cell surface markers (CD90, CD105, CD117, and Stro-1) within the remaining fibroblastic population of four patients. Figure 1a illustrates the distribution of the cell surface markers, based on the most abundant marker per population, color coded according to the termed dominant marker, with the co-expressed markers indicated, adding to the diversity of the individual populations. Similar to what has been reported in the past, we found CD90^{+} fibroblastic cells in the PCa tissues to be nearly double than that found in benign tissues [19, 20]. There was no statistical difference in benign and PCa in the CD105-dominant population. Expression of CD105 was further validated in 79 PCa and 16 benign tissues by immune-localization in a tissue array. In benign prostate tissues, CD105 immunohistochemical staining was primarily restricted to endothelial cells (Fig. 1b). In PCa however, CD105 was primarily detected in the endothelia and heterogeneously expressed in stromal fibroblastic cells. We could not establish a correlation of Gleason grade to the expression of stromal fibroblastic CD105. Interestingly, staining for a neuroendocrine marker, chromogranin A, revealed its expression circumscribed by CD105^{+} fibroblasts (Fig. 1c and Supplementary Figure S1). In the subset of six tissues that were positive for neuroendocrine differentiation, assessed by chromogranin A staining, stromal CD105 was also expressed in 83% of these same tissues; receiver operating characteristic (ROC) analysis provided an area under the curve (AUC) of 0.751 ($p = 0.0026$, Fig. 1d). The treatment status of these patients was not known. Next, we used the R2 analysis platform to calculate the correlation coefficient between CD105 to a panel of nine neuroendocrine genes in a transcriptomic analysis of 545 PCa patient tissues (Fig. 1e, $R = 0.703$ ($p = 1.4 \times 10^{-73}$) [21–23]. Taken together, the stromal fibroblastic CD105 population in tissues and primary cells was significantly associated with epithelial neuroendocrine differentiation (5).
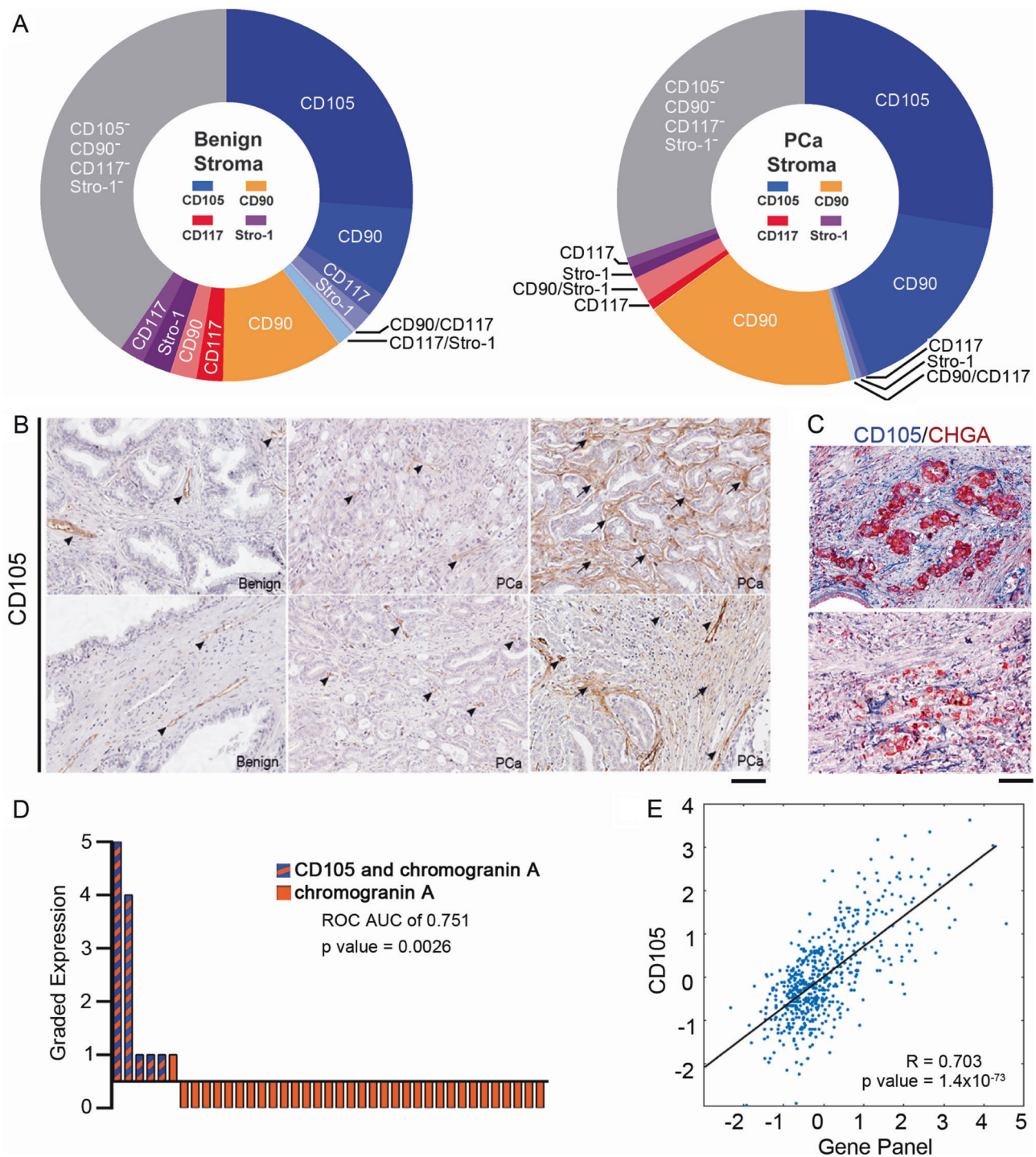
Cellular heterogeneity in carcinoma-associated fibroblasts determine its tumor supportive property

We next sought to confirm our finding from prostatectomy tissues with cultured CAFs and NAFs. Primary CAF cultures generated from prostatectomy tissues can promote the

expansion of established tumor epithelia [5, 24]. However, routine culturing of primary prostate CAF can lead to its loss of tumor-promoting potential. To characterize this observation, we compared primary cultured NAF, low passage CAF (3–7 passages) and high passage CAF (CAF^{HiP}, >8 passages) using FACS for CD90, CD105,

◀ **Fig. 1** Stromal CD105 expression is associated with neuroendocrine differentiation of the adjacent epithelia. **a** Donut charts show a representative patient stromal makeup from benign or cancer prostatectomy tissue. The relative percent is indicated for the stromal populations based on FACS, $n = 4$. The dominant population, determined by the marker of greatest intensity per cell, are colored with shades of: blue (CD105), gold (CD90), red (CD117), purple (Stro-1). The double, triple, and quadruple stained cell populations are shown as lighter shades among their dominant population. Gray indicates negative staining for CD105, CD90, CD117, and Stro-1. **b** Immunohistochemical staining of CD105 (brown) from representative core sections of tissue arrays counterstained with hematoxylin. Arrow heads indicate CD105-positive blood vessels and arrows indicate CD105-positive stromal fibroblast staining, $n = 94$. Scale bar represents 100 μm. **c** Representative serial sections from tissue cores stained for CD105 and chromogranin A, counterstained with hematoxylin, $n = 39$ paired tissues. A pseudo-colored overlay is shown to emphasize the localization of CD105-positive (blue) staining relative to chromogranin A positive staining (magenta). Scale bar represents 100 μm. **d** Waterfall plot indicates relative expression of epithelial chromogranin A (orange bars) and those that had co-expression of stromal CD105 (hatched orange and blue bars) on a graded scale of 0–5, where 5 was the greatest staining in paired cores, $n = 39$. **e** Scatter plot of the canonical correlation based on the R2 analysis platform between the neuroendocrine gene panel (AURKA, SCG3, MYCN, CGA, CGB, ENO2, NKX2.2, FOXA2) and CD105

CD117, and Stro-1. There was an overall statistical difference in the composition between NAF, CAF, and CAF^{HiP} populations (Fig. 2a, $p = 0.03$). Interestingly, the most abundant fibroblastic population in NAF and CAF was the CD90$^+$/CD105$^+$ population compared to the CAF^{HiP} ($p = 0.03$ and $p = 0.06$, respectively). In agreement with previous studies that prostatic fibroblasts can induce epithelial cell expansion [5], the xenografts with human CWR22Rv1 (22Rv1) PCa epithelia alone resulted in negligible tumors compared to tissue recombinant grafts with stromal fibroblastic cells (Fig. 2b). Interestingly, there was no statistical difference between tissue recombinants using NAF and CAF in the progression of the established tumor epithelia, although the CAF provided a distinct growth advantage to non-tumorigenic BPH1 epithelia over NAF under similar conditions (data not shown). Regardless, tissue recombinants of 22Rv1 and CAF^{HiP} resulted in tumor volumes larger than 22Rv1 epithelia alone ($p < 0.05$) but, significantly smaller than recombinants associated with NAF or CAF ($p < 0.001$ and $p < 0.0001$ respectively). Epithelial proliferation, as determined by Ki67 epithelial localization, was found to be greatest to least abundant in CAF > CAF^{HiP} > NAF-associated recombinants (Fig. 2c, d). However, CAF^{HiP}-associated tumors had the lowest expression of survivin, compared to NAF or CAF recombinant tumors (Fig. 2c, e). CAF-associated tumors were found to have significantly greater Ki67-expressing epithelia and reduced TUNEL staining, compared to NAF- or CAF^{HiP}-associated tumors. This corroborated the concept of population drift, resulting from extended culturing of primary cells.

Secreted frizzled-related protein 1 expression is elevated in CAF stromal cell populations

To identify the differences in paracrine mediators among the three stromal cell types, we performed RNA-sequencing and segregated the genes based on their expression pattern. We first compared CAF to CAF^{HiP}, as shown in the volcano plot comprises the top 200 differentially regulated genes (Fig. 3a). The top significantly upregulated genes were ependymin related 1 (EPDR1), lysyl oxidase (LOX), follistatin (FST), and SFRP1. Differential gene expression among CAF, CAF^{HiP}, and NAF was analyzed based on the combined ranked ratios of CAF/CAF^{HiP} and CAF/NAF. Candidate paracrine mediators (33 secreted genes, by gene ontology analysis from the top 200 differentially regulated genes) were plotted in a heat map, revealing nine genes expressed in both NAF and CAF, but not found in the CAF^{HiP} (Fig. 3b). Of the top significantly upregulated genes, only SFRP1 was co-expressed in both CAF and NAF populations. Presumably, paracrine mediators in the NAF and CAF, not expressed in CAF^{HiP}, enabled the observed tumor expansion in Fig. 2b. Therefore, the nine genes common to NAF and CAF populations drew our attention as potential CD105-associated mediators of tumorigenicity.

Stromal CD105-mediated SFRP1-induced PCa neuroendocrine differentiation

Next, a unique primary CAF line was identified to be spontaneously enriched in CD105 (CAF^{CD105en}, 99% of the population) compared to primary CAF samples from other patients (56% ± 10), that maintained its high CD105 expression through passaging. A set of CAF-related genes based on previous studies and our RNA-sequencing data were assessed in NAF, CAF, and the CAF^{CD105en} cells. MMP-1, MMP-3, Cox-2, tenascin C (TNC), and secreted frizzled-related protein 1 (SFRP1) were elevated in CAF more than 20-fold compared to NAF (Fig. 4a). The expression of SFRP1 and TNC was further elevated in CAF^{CD105en} compared to either NAF or CAF ($p < 0.001$). However, two-way ANOVA of the entire gene expression panel suggested that the CAF and CAF^{CD105en} were statistically similar. Notably, the traditional tumor-associated fibroblastic markers of alpha-smooth muscle actin, fibroblast activating protein (FAP), and IL-6 were not higher in the cultured CAF or CAF^{CD105en} compared to NAF.

With the goal of identifying a neuroendocrine differentiation promoting paracrine factor, we directly tested whether CD105 expression affected SFRP1 expression using a CD105 neutralizing antibody, TRC105. TRC105 blocked human CD105-mediated BMP2 activity without affecting TGF-β signaling (Supplementary Figure S2) [25]. The low SFRP1 expression in 22RV1 was not affected by
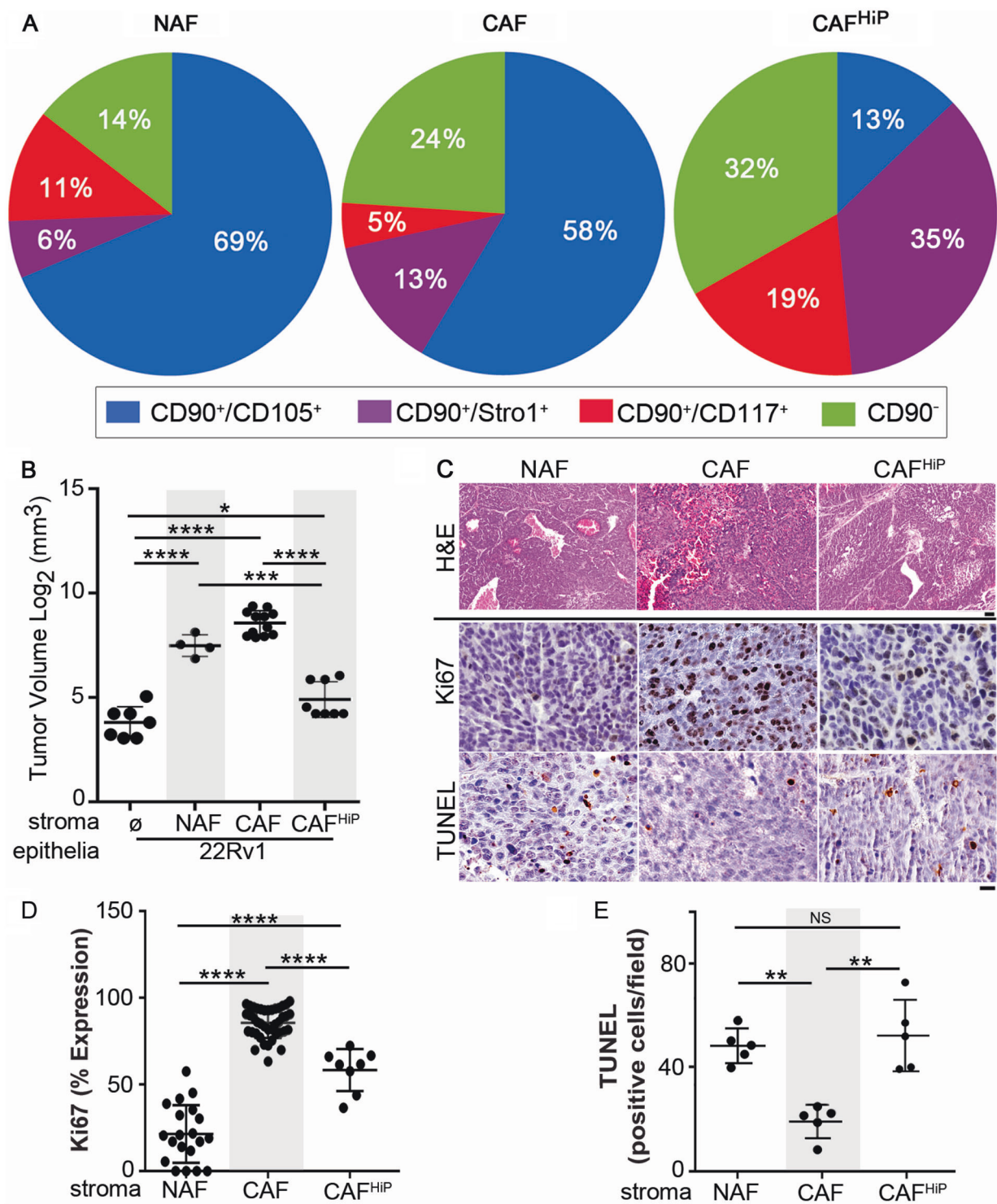
Fig. 2 Stromal heterogeneity dictates tumor progression. **a** Pie charts illustrate the relative ratio of the indicated stromal fibroblastic populations based on cell surface expression of the indicated markers: CD90$^+$/CD105$^+$ (blue), CD90$^+$/Stro-1$^+$ (purple), CD90$^+$/CD117$^+$ (red), and CD90$^-$ (green), $n > 3$. ANOVA analysis demonstrates NAF, CAF, and CAF^{HiP} have distinct populations ($p < 0.03$). **b** Scatter plot indicates individual tumor volume (log transformed) for tissue recombinant tumors made up of 22Rv1 epithelia with the indicated fibroblastic populations. $n > 4$. **c** Histology for representative recombinant tumor sections of 22Rv1 with the indicated fibroblastic populations are shown. H&E staining shows tumor morphology (scale bar represents 64 μm). Ki67 and TUNEL immune-localization, with hematoxylin nuclear counterstain (scale bar represents 32 μm), is shown, $n > 5$. **d** The scatter plot shows quantitation of percent expression for Ki67 immunohistochemical staining, $n > 8$. **e** The scatter plot shows quantitation of the number of TUNEL positive nuclei per field by immunohistochemical staining, $n > 5$. For all, error bars are mean ± SD, and p-values of <0.05 were considered statistically significant (*$p < 0.05$, **$p < 0.01$, ***P < 0.001, ****$p < 0.0001$)

TRC105, however TRC105 significantly downregulated SFRP1 in CAF^{CD105en} ($p < 0.0001$) (Fig. 4b). Furthermore, the knockdown of CD105 in CAF^{CD105en} by siRNA also resulted in decreased SFRP1 expression (Supplementary Figure S3). SFRP1 gene expression was found to be co-expressed with thrombospondin 1 (THBS1), platelet-derived growth factor-1 (PDGFC), tectonic family member 1 (TCTN1), and zinc finger protein 449 (ZFN449), based on TCGA gene association query (Supplementary Figure S3) [26]. Of the four SFRP1 regulated genes, PDGFC, sonic hedgehog (target of TCTN1), and THBS1 are associated with tumor neuroendocrine differentiation. There was further evidence of the role of SFRP1 in neuroendocrine differentiation of PCa in the TCGA, where SFRP1 gene amplification was associated with neuroendocrine differentiation (Supplementary Figure S3). To test the role of SFRP1 on epithelial neuroendocrine differentiation more comprehensively, we treated cultured 22Rv1 with recombinant SFRP1 to find a significant induction of nine PCa neuroendocrine differentiation genes [15] in a dose-dependent manner ($p < 0.001$; Fig. 4c). However, the same doses of SFRP1 had no effect on epithelial proliferation (Supplementary Figure S3). To further confirm the neuroendocrine response of stromal-derived SFRP1 on epithelia, we knocked down SFRP1 by 10-fold using siRNA in CAF^{CD105en} and used this conditioned medium to treat 22Rv1. The knockdown of SFRP1 significantly decreased the neuroendocrine differentiation gene panel without affecting proliferation, compared to control transfected CAF^{CD105en} cells ($p < 0.0001$; Fig. 4d and Supplementary Figure S3). To further confirm this mechanism in an alternative cell line, we treated C4-2B cells with enzalutamide in the presence of conditioned media from wild-type mouse fibroblasts or CRISPR/Cas9 CD105-knockout mouse fibroblasts to measure the expression of the neuroendocrine differentiation gene panel ($p < 0.0001$, Fig. 4e,
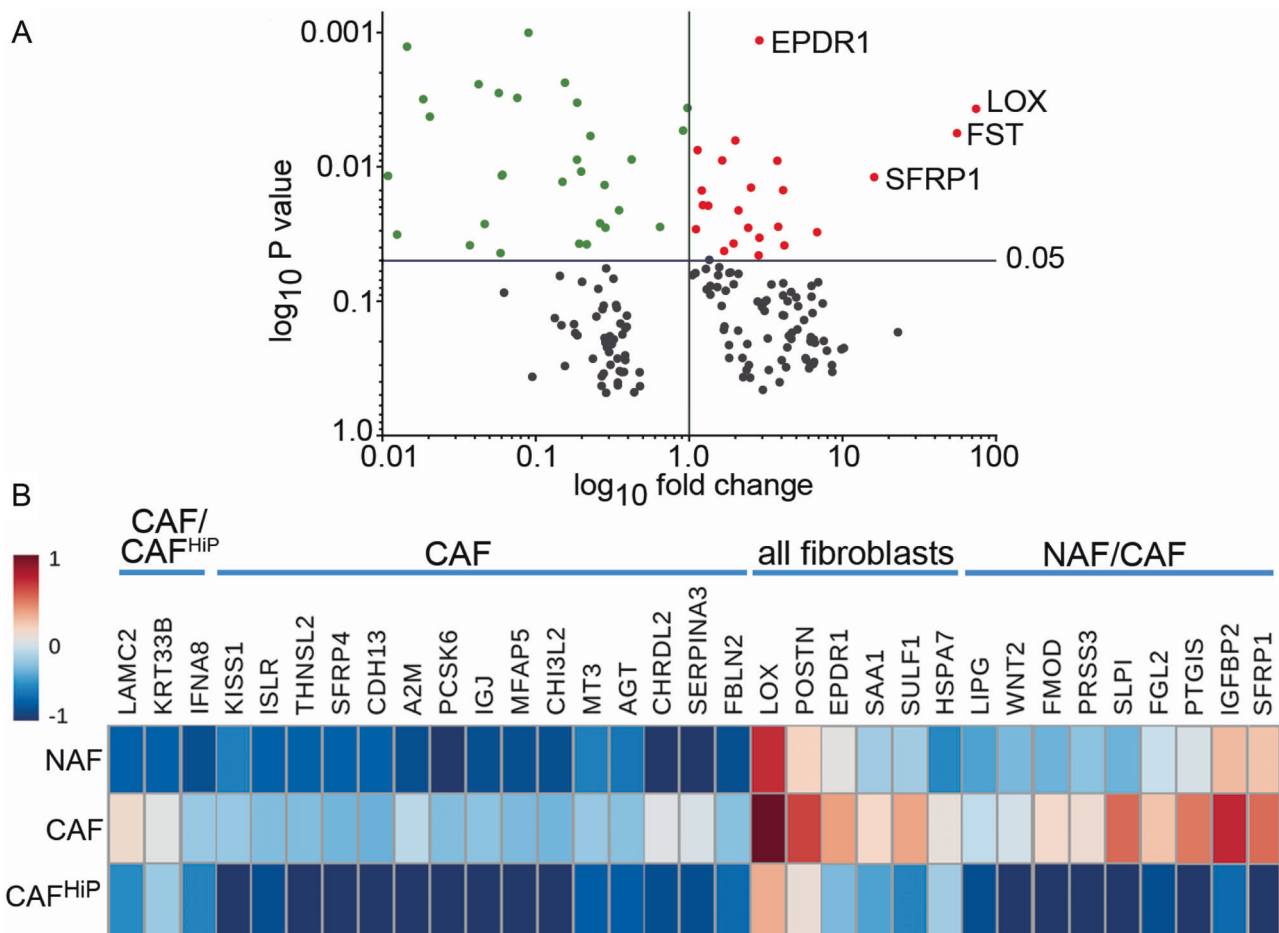

Fig. 3 Differential gene expression in NAF, CAF, and CAF^{HiP} stromal fibroblasts. a The top 200 differentially expressed genes identified by RNA-sequencing were plotted in a volcano chart to compare the ratio of CAF^{HiP} to CAF. The effect size ratio was set to 1 indicating less effect below this threshold. Genes in the upper right quadrant (red) are considered significant with an effect >1. Genes in the upper left quadrant (green) were considered significant with less effect. b Among the top 200 differentially expressed genes, 33 coded for secreted proteins, illustrated in the heat map following log transformation. The labels above the gene names highlight expression in NAF, CAF, and CAF^{HiP}
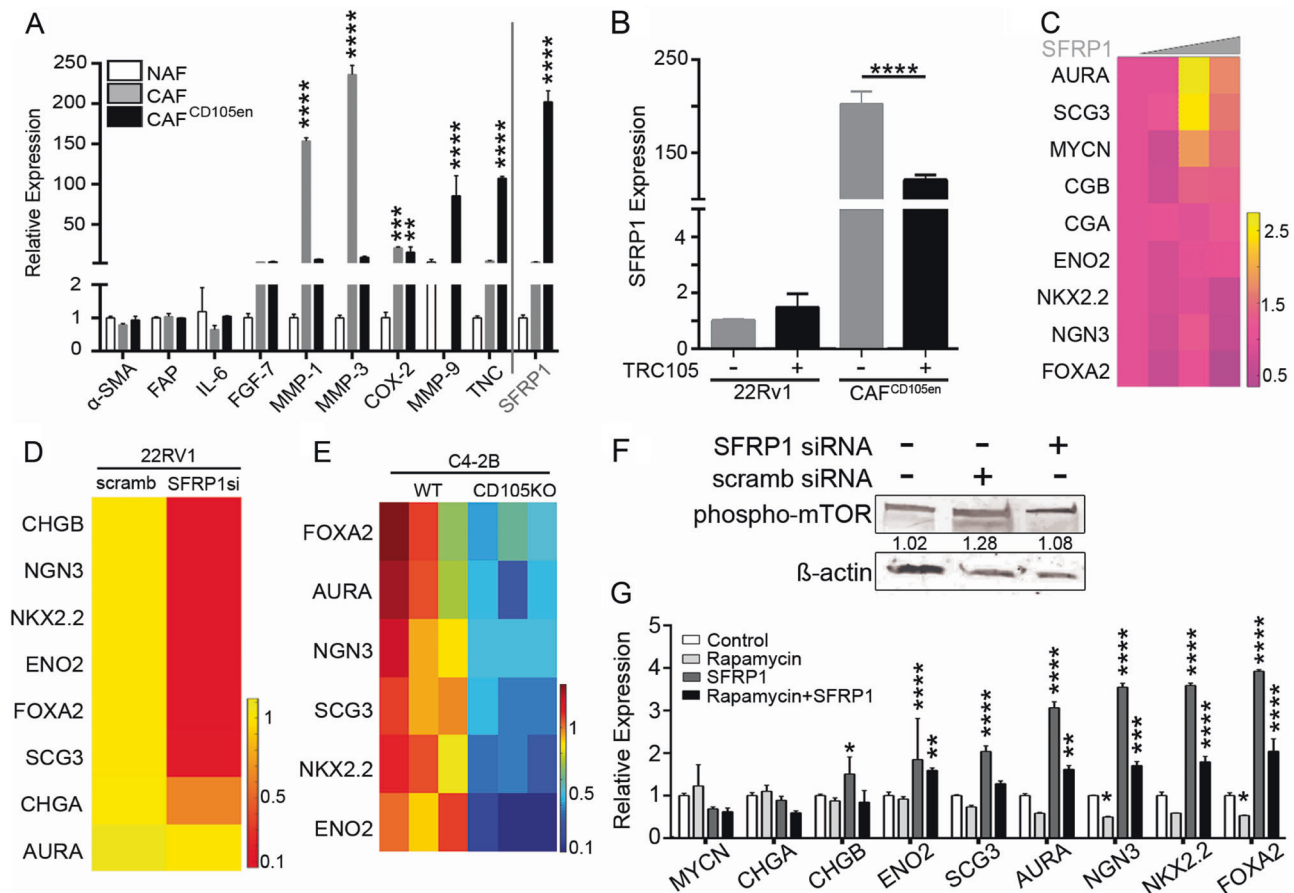
Fig. 4 Androgen axis inhibition mediates paracrine SFRP1-mediated neuroendocrine differentiation. **a** Relative mRNA expression for the indicated genes is graphed for NAF (white), CAF (gray), and CAF^{CD105en} (black) as mean ± SD, $n = 3$. Primer sequences are listed in Supplementary Table S1. **b** Bar graph shows relative SFRP1 mRNA expression in human 22Rv1 and CAF^{CD105en} regulated by TRC105 compared to IgG (control) treatment, $n > 3$. **c** Heat map shows the relative expression for the neuroendocrine gene panel in 22Rv1 cells, normalized to GAPDH, when treated with 0, 0.01, 0.1, and 1 μg/ml SFRP1, $n = 3$. Gradient scale from 2.5-fold increase (yellow) to 0.5-fold decrease (purple) indicates gene expression changes compared to control. **d** Heat map shows the relative expression for the neuroendocrine gene panel in 22Rv1 cells, normalized to β-actin, when treated with enzalutamide in combination with conditioned media from CAF-nucleofected with scramble or siRNA against SFRP1, $n = 3$. Gradient scale from 1-fold increase (yellow) to 0.1-fold decrease (red) indicates gene expression changes compared to scramble control. **e**

Heat map shows the relative expression for the neuroendocrine gene panel in C4-2B cells, normalized to β-actin, when treated with enzalutamide in combination with conditioned media from wild-type fibroblasts or CD105-knockout fibroblasts, $n = 3$. Gradient scale from 1-fold increase (red) to 0.1-fold decrease (blue) indicates gene expression changes compared to wild-type conditioned media. **f** Immunoblot shows 22Rv1 cell protein expression for phosphorylated-mTOR and β-actin as the loading control, treated with control media or CAF-nucleofected with scramble or siRNA against SFRP1 as indicated for 72 h. The ratio of phospho-mTOR/β-actin is shown. **g** Bar graph shows the relative gene expression for the indicated neuroendocrine differentiation genes in 22Rv1 cells treated with rapamycin (1 μM) and/or SFRP1 (0.1 μg/ml) for 72 h, $n = 3$. * indicates significant gene expression compared to control. For all, error bars are mean ± SD, and p-values of <0.05 were considered statistically significant (**$p < 0.01$, ***$p < 0.001$, ****$p < 0.0001$)

Supplemental Figure S3). After confirming this mechanism at the transcriptional level, 22Rv1 were again treated with conditioned medium from CAF-nucleofected with siRNA against SFRP1 compared to scramble control, which resulted in elevated mTOR phosphorylation (Ser 2448, associated with mTORC1 activation) (Fig. 4f) [27, 28]. Furthermore, 22Rv1 were treated with combinations of recombinant SFRP1 and/or an mTOR inhibitor, rapamycin. The SFRP1-induced neuroendocrine gene panel was restored to near control levels with the addition of rapamycin, in support of the role of SFRP1 in neuroendocrine

differentiation via mTOR signaling, in the absence of any effect on epithelial cell viability (p-value < 0.0001, Fig. 4g, Supplemental Figure S3). Fibroblast-derived SFRP1 was necessary and sufficient for epithelial neuroendocrine differentiation.

ADT induces neuroendocrine differentiation in a stromal CD105-dependent manner

To better understand the regulation of CD105 in both fibroblasts and epithelia, we generated 3D co-cultures with
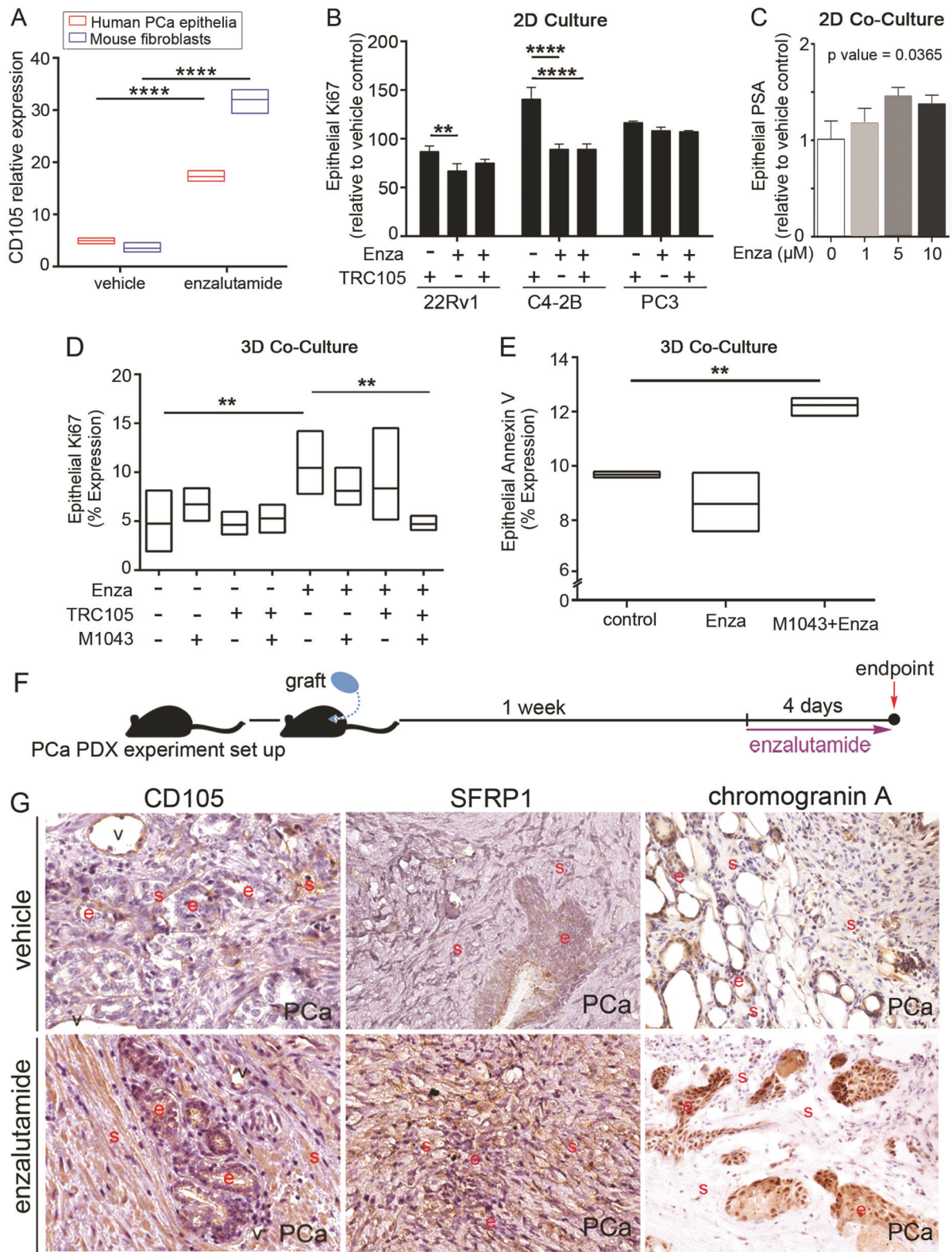
human 22Rv1 and mouse wild-type prostatic fibroblasts. As patients can develop neuroendocrine PCa when undergoing ADT, we used enzalutamide to reproduce this physiological state. Treatment with enzalutamide resulted in a threefold increase in CD105 cell surface expression in epithelial and fibroblastic populations by FACS analysis, compared to

Fig. 5 Antagonizing the androgen axis increases CD105 with elevated neuroendocrine differentiation. **a** CD105 expression in human epithelial (22Rv1) and wild-type mouse prostatic fibroblastic cells in a 3D co-culture model is regulated by enzalutamide treatment, as determined by FACS analysis, $n = 3$. **b** Epithelial proliferation of prostatic epithelia 22Rv1, C4-2B, and PC3 was determined by FACS analysis for Ki67$^+$ cells in the presence and absence of TRC105 (1 µg/ml) and enzalutamide (5 µM), $n = 3$. **c** Epithelial PSA expression is shown from a 2D co-culture of 22Rv1 with wild-type mouse prostatic fibroblasts after a 16 h treatment with indicated enzalutamide doses in hypoxia, $n = 3$. **d** Epithelial proliferation of human 22Rv1, in a 3D co-culture model with mouse prostatic fibroblasts, were analyzed for double EpCAM$^+$ and Ki67$^+$ expression by FACS. The cultures were treated with TRC105, M1043, and/or enzalutamide for 72 h, $n > 3$. **e** Epithelial cell death of human 22Rv1, in a 3D co-culture model with mouse prostatic fibroblasts, were measured for double EpCAM$^+$ and Annexin V$^+$ expression by FACS. The cultures were treated with M1043 and/or enzalutamide for 72 h, $n = 3$. **f** In a PDX model, the mice were xenografted with untreated human prostatectomy tissue under the renal capsules. Tissues grew for 1 week and then the mice were treated with either vehicle or enzalutamide for 4 days. **g** Immunohistochemical localization of CD105, SFRP1, or Chromogranin A in benign or PCa tissues were counterstained with hematoxylin. Red letters were used to highlight positive staining in blood vessels (v), epithelia (e), and stroma (s), $n > 5$. Scale bar represents 100 µm. For all, error bars are mean ± SD, and p-values of <0.05 were considered statistically significant (*$p < 0.05$, **$p < 0.01$, ***$p < 0.001$, ****$p < 0.0001$)

vehicle (Fig. 5a). To test the effect of ADT and CD105 inhibition directly on epithelial cells, we treated 22Rv1, C4-2B, or PC3 monolayer cultures with enzalutamide in the presence or absence of TRC105. Ki67 expression was measured by FACS. We found that enzalutamide effectively downregulated the proliferation of AR expressing 22Rv1 and C4-2B cells ($p < 0.01$, Fig. 5b). The administration of TRC105 had little proliferative effect in the presence or absence of enzalutamide treatment of 22Rv1 or C4-2B cells. Further determination of epithelial cell viability by MTT assay confirmed reduced viability of the cells with enzalutamide treatment (Supplementary Figure S4). TRC105 did not impact cell viability. The PC3 cells, with no androgen receptor expression, were predictably insensitive to either enzalutamide in the presence or absence of TRC105. In light of the observed epithelial proliferation with enzalutamide, we tested epithelial prostate-specific antigen (PSA) expression by real-time PCR in co-cultured 22Rv1 or C4-2B with wild-type mouse fibroblasts in the presence of enzalutamide. The co-cultured 22Rv1 demonstrated elevated PSA expression with enzalutamide in a dose-dependent manner ($p < 0.05$, Fig. 5c). Whereas, PSA expression was significantly decreased in co-cultured C4-2B cells given enzalutamide ($p < 0.05$, Supplemental Figure S4). In line with elevated PSA expression by 22Rv1 when co-cultured with wild-type fibroblasts, in 3D co-cultures of the same cells, enzalutamide caused a doubling of epithelial proliferation when normalized to vehicle control ($p < 0.01$, Fig. 5d). We utilized the species differences to target the

epithelia with the human-specific CD105 neutralizing antibody, TRC105, or fibroblasts with the mouse-specific CD105 neutralizing antibody, M1043 [25]. At the dose used for this study (1 µg/ml), we found no cross-species reactivity of the two antibodies or alterations of TGF-ß signaling (Supplementary Figure S2). The co-cultures were treated with enzalutamide in the presence or absence of TRC105 and/or M1043. The resultant changes in epithelial proliferation were quantitated by FACS analysis for Ki67 expression of EpCAM$^+$ cells. Treatment with either M1043 or TRC105 alone did not change epithelial proliferation compared to IgG control. However, combining enzalutamide with both M1043 and TRC105 reduced epithelial proliferation, compared to enzalutamide alone ($p < 0.01$). In support of fibroblastic expression of CD105 eliciting the dominant effect, M1043 (in the absence of TRC105) with enzalutamide resulted in a significant increase in epithelial cell death, measured by EpCAM$^+$/annexin V staining, compared to control or enzalutamide ($p < 0.01$, Fig. 5e). Thus, CD105$^+$ fibroblastic population is consequential to castrate resistance due to cell-specific effects on epithelial proliferation and death in the context of ADT.

Next, we attempted to validate the associated increase in CD105 following ADT using PCa patient-derived xenograft (PDX) models. Treatment-naive PCa tissues were grafted in the sub-renal capsule and allowed to vascularize for 1 week before treatment with either vehicle or enzalutamide for 4 days (Fig. 5f). The grafts were harvested and evaluated for the expression of CD105, SFRP1, and chromogranin A. As before, CD105 was predominantly immune-localized on the vascular endothelia in the absence of enzalutamide treatment (Fig. 5g). However, enzalutamide treatment resulted in the upregulation of CD105 immuno-localization in both epithelial and CAF populations with SFRP1 upregulation in the PDX tissues. Double immunohistochemical staining indicated CD105$^+$ fibroblasts proximal to chromogranin A$^+$ epithelial cells in the enzalutamide treated mice, compared to vehicle treated mice (Supplementary Figure S5). Together, the data suggested that blocking the androgen axis was associated with elevated CD105 expression and PCa neuroendocrine differentiation.

Antagonizing CD105 can sensitize PCa to androgen-targeted therapy

To determine whether antagonizing CD105 sensitizes CRPC to ADT, we utilized an orthotopic castrate-resistant tissue recombinant model comprised of human CAF and 22Rv1. The tumors were expanded for 3 weeks prior to castrating the mice. A subset of mice was also treated with enzalutamide, in the presence or absence of TRC105 for an additional 3 weeks to mimic secondary treatment after castration equivalent therapies have failed. Notably,
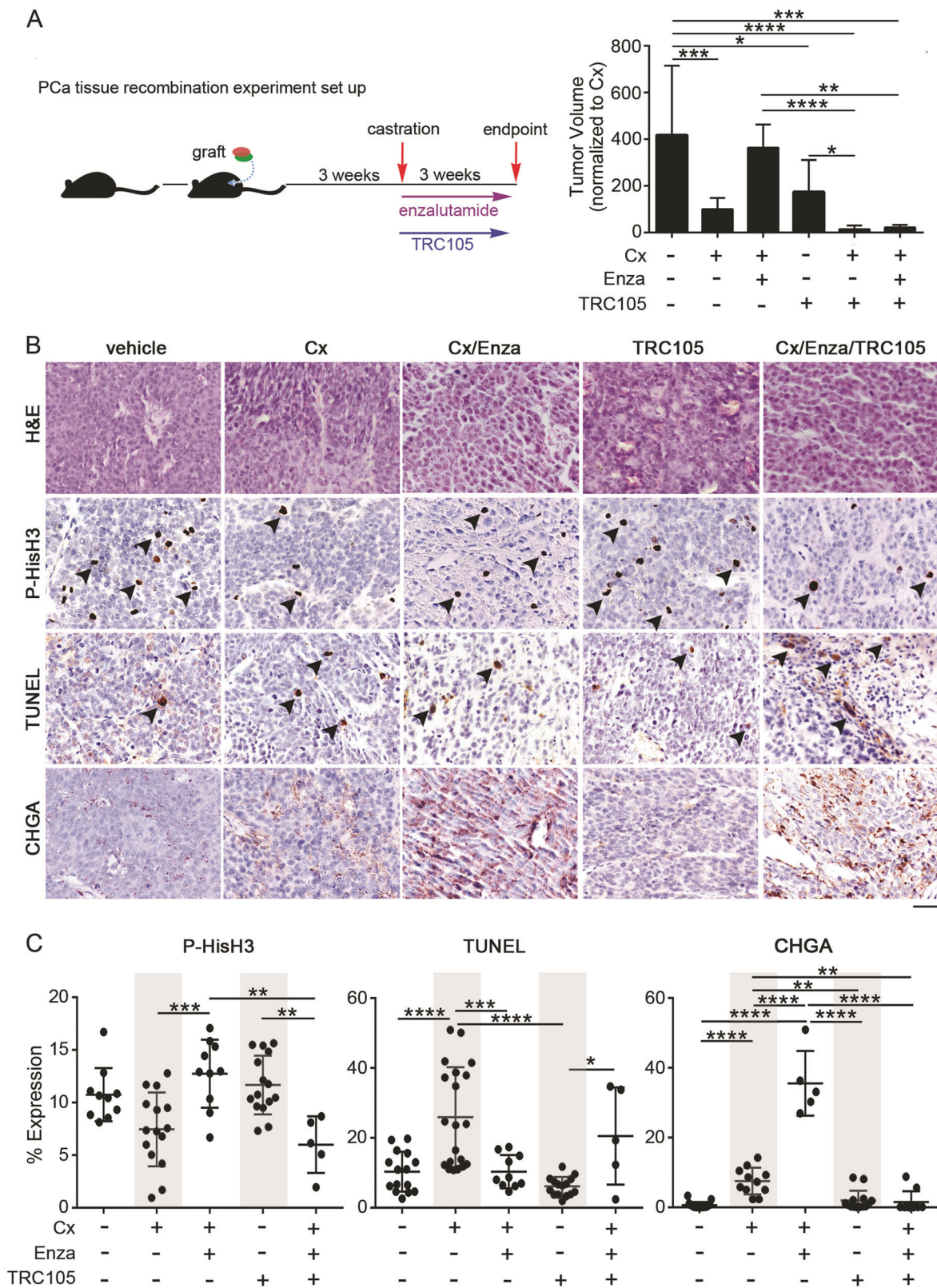
Fig. 6 Antagonizing the androgen axis and CD105 reduced tumor growth and neuroendocrine differentiation. **a** Mice were orthotopically grafted with tissue recombinants of 22Rv1 and CAF. The mice were castrated, treated with TRC105, and/or enzalutamide. Bar graph shows tumor volumes normalized to castrated (Cx) mice. **b** H&E staining was followed by immune-localization for phosphorylated-histone H3 (P-HisH3), TUNEL, and chromogranin A (CHGA). Scale bar represents 32 μm. **c** The scatter plots show the mitotic (PHis-H3), cell death (TUNEL), and chromogranin A positive staining indexes, mean ± SD, $n > 5$. For all, error bars are mean ± SD, and p-values of <0.05 were considered statistically significant (*$p < 0.05$, **$p < 0.01$, ***$p < 0.001$, ****$p < 0.0001$)

TRC105, a human-specific CD105 antagonist, does not impact host vascularization of the xenografts. Castrated mice had reduced tumor volumes compared to controls ($p < 0.001$; Fig. 6a). Histologic measure of mitosis by phosphorylated-histone H3 was unchanged, however castration resulted in an expected increase in TUNEL staining ($p < 0.0001$; Fig. 6b, c). In this CRPC xenograft model, the castrated mice given enzalutamide had tumor volumes and histologic measures of cell turnover statistically comparable to control intact mice. Mice treated with TRC105 alone had tumors smaller than vehicle ($p < 0.05$), with no notable changes in histology, proliferation, or cell death, compared to control. As patients on enzalutamide are normally at a castrate state, we combined castration with enzalutamide and compared the tumors to that generated following the addition of TRC105. We found substantially reduced tumor size with the addition of TRC105 compared to either control or castrated-enzalutamide treatment alone ($p < 0.001$ and $p < 0.01$, respectively). Castrated mice given TRC105 resulted in the smallest tumor volume compared to control ($p < 0.0001$), with tumors too small to section for reliable histologic analysis. The marked chromogranin A staining associated with ADT (castrated mice given enzalutamide), was reduced by the added administration of TRC105 (p-value < 0.0001). Together, blocking the androgen axis was associated with increased CD105 contributing to neuroendocrine differentiation of PCa via fibroblast-derived paracrine SFRP1 (Fig. 7).

Discussion

This study identifies the role of the CD105$^+$ fibroblastic population in the heterogeneous stroma initiating a novel paracrine SFRP1 signaling axis critical to castrate-resistant PCa. We used a recognized change of the loss of tumor potentiation resulting from extended culturing of primary CAF to identify a mechanism for paracrine PCa differentiation. For the first time, we identified that CD105/BMP signaling is upregulated in response to ADT using mouse models. We found that stromal CD105 expression was associated with prostatic epithelial neuroendocrine differentiation in patient tissues and a mechanistic role for SFRP1 in the process (Fig. 7). Ultimately, we discovered that combining androgen-targeted therapy with a CD105 neutralizing antibody markedly reduced neuroendocrine differentiation and resultant tumor size in a model of therapy-resistant disease.

Stromal–epithelial interactions have defined organ development and cancer progression. We identified a subpopulation of stromal fibroblastic cells that regulate androgen sensitivity of PCa epithelia. Previous studies have demonstrated the importance of CD105 in PCa progression [29]. However, the explicit decrease of CD105 in the CAF^{HiP} cells initiated further interrogation of CD105 as it was similarly expressed in both NAF and CAF as well as fibroblasts from benign and PCa tissues. Validation of this culturing-associated population drift in CAF^{HiP} also included reduction of the CD90$^+$ population, reported to be a hallmark of tumor-inductive CAF [19, 20]. FACS analysis enabled examination of the stromal population makeup on a per cell basis, not just a total change in expression (Figs. 1 and 2). FACS analysis of benign and PCa tissues supported the previous reports regarding elevated CD90$^+$ fibroblastic populations in CAF [19, 20]. There is precedence for tumor-associated stromal cells to be derived from proliferative endothelia supporting breast cancer progression [30, 31]. The identification of the samples that exhibited neuroendocrine features and adjacent CD105$^+$ fibroblasts directed us to further examine the role of CD105 in the context of ADT.

The biologic heterogeneity of advanced PCa is attributed to its resistance to ADT [32]. Although not mutually exclusive, therapeutic resistance can be a result of a population of cells that are selected by the attrition of sensitive ones or through an active acquisition of adaptive features [33]. These models are based on cell-autonomous mechanisms of resistance. Although NAF and CAF were originally
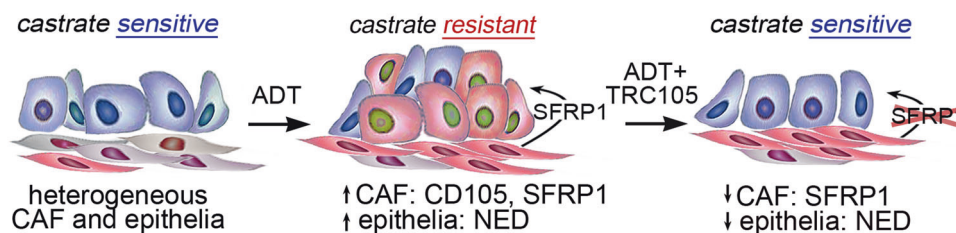

Fig. 7 Antagonizing the androgen axis increases CD105 and SFRP1 expression with elevated neuroendocrine differentiation. Diagram shows the evolution of prostate cancer (PCa) stroma and epithelia. Castrate sensitive PCa epithelia (blue top layer of cells) and stromal fibroblasts (bottom elongated layer of gray and CD105$^+$ red cells) are both initially heterogeneous. After treatment with ADT, the epithelia and stroma express more CD105 (red). ADT induces SFRP1 secretion by fibroblasts that signal to the adjacent epithelia to induce neuroendocrine differentiation. The combined treatment with ADT and CD105 inhibition via TRC105 resulted in SFRP1 downregulation and reduced epithelial neuroendocrine differentiation in promoting castrate sensitivity

coined for their respective lack of or capacity to initiate tumorigenesis [3–5], when combined with established cancer epithelia, we found their shared ability to promote expansion of 22Rv1 cells (Fig. 2). We used a recognized decrease in tumorigenicity by extended culturing of CAF to identify the nature of the drift in fibroblastic populations. Specific upregulation of the CD105$^+$ fibroblastic population in response to ADT-mediated neuroendocrine differentiation of PCa epithelia in a paracrine manner downstream of SFRP1 (Figs. 3 and 4). SFRP1, originally recognized to antagonize Wnt ligands, has previously been associated with epithelial branching morphogenesis in the prostate [34, 35]. SFRPs have more recently been shown to have a role in promoting Wnt diffusion and correlated with tumor progression [36–38]. Importantly, SFRP1 and SFRP2 are also reported to have Wnt-independent effects [39], and the capacity to inhibit androgen receptor transcriptional activity [40, 41]. The ability for recombinant SFRP1 to induce neuroendocrine features in PCa cells, inclusive of aurora kinase, n-myc, and secretogranin-3, supported its Wnt-promoting activity (Fig. 4). Stromal CD105 expression was associated with prostatic epithelial neuroendocrine differentiation, in patient tissues as well as the PDXs when administered ADT (Figs. 1 and 5). Consequently, we found that combining ADT with TRC105 dramatically reduced tumor size in a model of ADT resistant disease (Fig. 6). The acute changes in the PDX model correlated with the longer-term tissue recombinant xenograft model (6 weeks). These findings go beyond the known association of elevated vascular CD105 with poor PCa prognosis, in providing a mechanism for the paracrine-mediated fibroblast CD105-SFRP1 response to ADT [42]. Although, we focus on stromal SFRP1 eliciting neuroendocrine differentiation on prostatic epithelia, other differentially expressed genes found in our sequencing analysis in CAF vs NAF or CAF^{HiP} may also have roles as has been demonstrated by IGFBP-2 [43]. The genes in our circus plot (PDGF, TCTN1, ZNF449, and THBS) are reported to be co-expressed with SFRP1 and known to be involved in neuroendocrine differentiation (Supplemental Figure S2) [44, 45]. However, there is no claim that these genes are necessary or sufficient to induce neuroendocrine differentiation like SFRP1. The relation of the other genes in the circus plot to CD105 is yet to be determined. Our current work provides the foundation for subsequent studies to provide a well-rounded understanding of prostatic neuroendocrine differentiation.

The strategy to combine ADT and CD105 antagonism is an example of synthetic lethality. We identified a mechanism for paracrine-mediated CRPC and addressed a means for its therapeutic resolution. Since ADT promoted CD105 expression in both fibroblastic and epithelial cells (Fig. 5), the cells are more susceptible to its antagonism. The roll of CD105 in fibroblasts and epithelia are likely quite different,

as the epithelia do not respond to ADT by expressing SFRP1 nor was the epithelia able to develop resistance on its own. We do acknowledge the potential for CD105 effects outside of the scope of this study. Notably, elevated PSA expression in 2D co-cultures of 22Rv1 with wild-type fibroblasts treated with enzalutamide corresponded with elevated proliferation in 3D co-cultures of 22Rv1 and wild-type fibroblasts treated with enzalutamide. A similar phenomenon has been seen in patients, where PSA flares result from enzalutamide treatment [46]. As demonstrated in our 3D co-cultures, inhibition of both stromal and epithelial CD105 was necessary to suppress the proliferative effects of ADT on PCa epithelia. However, TRC105 had little direct effect on the proliferation or viability of mono-cultured PCa epithelia in the presence or absence of enzalutamide (Fig. 5 and Supplemental Figure S2), much like the lack of the progression-free survival change in CRPC patients given single agent TRC105 [47]. Overall these findings support the idea that simultaneous targeting of both stromal and epithelial cell compartments with TRC105 and ADT may provide a better therapeutic option for CRPC patients, however its clinical validation is required.

Materials and methods

Cell culture and reagents

Primary fibroblasts were grown out of prostatectomy specimens from Cedars-Sinai Medical Center or the Greater Los Angeles Veterans Affairs under respective Institutional Review Boards [9, 48]. The designation of NAF and CAF were determined by tissue recombination with BPH1 non-tumorigenic prostatic epithelia [3–5]. Mouse primary fibroblasts were grown out of prostate specimens using the same method as human fibroblasts. Conditioned media was generated by plating NAF or CAF at a density to reach confluence at the end of 72 h, at which time the cultured media was centrifuged and supernatant used fresh or stored at −80 °C [7, 48]. Target cells were treated with 50% conditioned media in combination with 50% control media. Viability assays were done using MTT reagent (M6494, Life Technologies) as directed.

Generation of CD105-knockout mouse fibroblasts

293T cells were transfected at a confluence of 70% using BioT (Bioland, CA), Cas9 vector (52962, Addgene), pCMV-dR8.91 (8455, Addgene), pCMV-VSVG (8454, Addgene) following the BioT protocol per manufacturer's protocol with a 9:1 ratio of Delta 8.9 to VSVg. Twenty-four hours after transfection, the medium was replaced with only 50% of the volume and virus was collected after 48 and 72 h and filtered

with a sterile 0.45 µM sterile syringe filter. Target wild-type mouse fibroblasts were seeded in 6-well plates at 200,000 cells per well. Virus was added with Polybrene (5 µg/ml, Sigma, MA) to the cell suspension at different ratios for a total of 2 ml 1:1, 1:5, 1:10, 1:100, 1:1000 and an uninfected control. 48 h after infection, virus was replaced with 2 ml of fresh medium. Selection was performed using blasticidin (5 µg/ml). The well which had a 10% infection ratio was selected to ensure one infection per cell.

Once the mouse fibroblasts stably expressed CAS9, an IDT gblock was designed with the sequence: AAGGTCGGGCAGGAAGAGGGCCTATTTCCCATGATTCCTTCATATTTGCATATACGATACAAGGCTGTTAGAGAGATAATTAGAATTAATTTGACTGTAAACACAAAGATATTAGTACAAAATACGTGACGTAGAAAGTAATAATTTCTTGGGTAGTTTGCAGTTTTAAAATTATGTTTTAAAATGGACTATCATATGCTTACCGTAACTTGAAAGTATTTCGATTTCTTGGCTTTATATATCTTGTGGAAAGGACGAAACACCGGTTTTAGAGCTAGAAATAGCAAGTTAAAATAAGGCTAGTCCGTTATCAACTTGAAAAAGTGGCACCGAGTCGGTGCTT, Single-cell clones were selected, grown out, and verified with FACS.

3D organotypic co-culture

A modified version of the 3D organotypic co-culture system was generated in collagen matrix. Gels were prepared by mixing five volumes of rat tail collagen I with two volumes of matrigel (NCI), one volume of 10x DMEM medium (GE Healthcare Life Sciences), and one volume of FBS (Atlanta Biologicals), 22Rv1 and primary mouse prostatic fibroblasts were combined in a 1:3 ratio [49]. Nylon squares were coated with collagen and placed on metal grids in a 6-well plate. Gel plugs (150 µl) were transferred onto the nylon squares, media was added to the level of the nylon mesh and incubated at 37 °C with 2% O_2. The cells were expanded in the matrix for 72 h, to be subsequently dissociated with collagenase and dispase for FACS analysis.

FACS analysis

FACS experiments were performed with eBiosciences antibodies: anti-human Stro-1-FITC (340105), anti-human CD90-PE (12-0909-42), anti-human CD105-APC (17-1057-41), anti-mouse CD105-APC (17-1051-82), anti-human CD117- PE-Cy5 (15-1178-41), anti-human Ki67-PECy7 (25-5699-41), anti-human EpCAM-FITC (53-8326-41), and anti-human EpCAM-PE (12-9326-41); and BD antibody: anti-human Annexin V (BD 556422). EpCAM (130-061-101, Miltenyi Biotec) and CD45 (130-045-801, Miltenyi Biotec) beads were used to negatively select for epithelial and immune cells, respectively, prior to FACS. BD LSRII was used to collect the data for analysis using FlowJo software v10.3. EpCAM$^+$ cells were gated for measuring epithelial CD105, Annexin V, or Ki67 expression in 3D co-cultures.

Animal studies

Male beige/SCID mice (Envigo), 6–8 or 10–12 weeks old, were used for sub-renal capsule or prostatic orthotopic grafting, respectively, as previously described [3, 18]. In accordance with institutional animal care and use committee approval, 2×10^5 22Rv1 cells and 6×10^5 stromal cells were suspended in 20 µl type I collagen to be grafted into the sub-renal capsule of mice, randomized with equal numbers to each treatment group without blinding, castrated after 7 days and sacrificed 21 days after castration. For orthotopic xenografts, mice were castrated after 3 weeks, they were treated three times weekly with enzalutamide (1 mg/mouse oral gavage) and/or TRC105 (50 µg/mouse i.v.) and killed 21 days after castration. Tumor volume was calculated using the modified ellipsoid formula $volume^3 = \pi/6 \times (width)^2 \times length$. For PDX models, prostatectomy tissues were xenografted into the sub-renal capsules and mice were treated after 1 week with enzalutamide.

Statistical analysis

FACS comparisons were normalized with arcsine square root transformation and then followed with ANOVA analysis. After log transformation, a Student's t-test was used to compare fibroblastic populations. Relative expression within each group of FACS data was plotted with Prism (GraphPad software) v6.07 using the pie or donut chart features.

For the RNA-seq data, raw sequencer data was processed using Illumina's RTA and CASAVA pipeline software, which includes image analysis, base calling, and sequence quality scoring. Moreover, we analyzed the RNA-seq data with our transcriptome analysis pipeline, which uses the Tophat software package for performing gapped alignments against the reference genome, DESeq for detecting differential gene expression. The log-fold change and a noise filter of minimum number (2) of FPKM for a gene were used to identify differentiated genes. The complete data set was uploaded in the GEO repository, accession # GSE99744. For the volcano plot, the top 200 genes among the RNA-sequencing data comparing CAF^{HiP} and CAF groups were analyzed using the grouped volcano plot feature with Prism. For the heat map, we pulled out the top 33 secreted genes among RNA-sequencing data, ratio values were generated for CAF/CAF^{HiP} and CAF/NAF gene values. Next, the ratio values were ranked for each ratio value among all the genes analyzed, with the highest value having a rank of 1. The ranks of CAF/CAF^{HiP} and CAF/NAF ratio values were summed. The sum values of the two ranks were then ranked. The

lowest sum value had the lowest rank, which inversely correlated with the most significant gene expression. MATLAB was used for heat map creation with gene-wise hierarchical clustering. Average linkage and Euclidean distances were calculated un-supervised. Two-way ANOVA analysis over all genes indicated statistically significant variations in expression patterns.

cBioPortal was used to check SFRP1 mutation, deletion, and amplification frequency and correlations across publicly available data sets generated by the TCGA Research Network: http://cancergenome.nih.gov/ as described previously [50, 51]. Multiple comparisons for in vitro data were evaluated with one-way or two-way analysis of variance (ANOVA). The tumor data was analyzed using one-way ANOVA for multiple comparisons. Results were expressed as individual data points or as the mean ± S.D. p-Values of <0.05 were considered statistically significant. Relative expression within each group of FACS data was plotted with Prism software using the pie or donut chart features. The concordance of stromal CD105 population and epithelial chromogranin A expression was measured with receiver operating characteristic (ROC) curve and the area under the ROC curve (AUC). The p-value for AUC (c-statistic) was determined with Mann–Whitney U test. All calculations were performed with ROC package in R. Multiple comparisons for in vitro data were evaluated with one-way or two-way analysis of variance (ANOVA). The tumor data were analyzed using one-way ANOVA for multiple comparisons.

Additional materials and methods can be found in the electronic supplementary material.

Author contributions Conceptualization, MK, VRP-H, and NAB; Methodology and Project Administration, MK and VRP-H; Investigation, MK, VRP-H, AM, SH, KR-R, MT, RM, SB, BS, PA, FD, and BA; Formal analysis, DH, JZ; Writing, MK, VRP-H, and NAB; supervision and funding, NAB.

Compliance with ethical standards

Conflict of interest The authors declare that they have no conflict of interest.

References

1. Bhowmick NA, Chytil A, Plieth D, Gorska AE, Dumont N, Shappell S, et al. TGF-beta signaling in fibroblasts modulates the oncogenic potential of adjacent epithelia. Science. 2004;303:848–51.

2. Ayala G, Tuxhorn JA, Wheeler TM, Frolov A, Scardino PT, Ohori M, et al. Reactive stroma as a predictor of biochemical-free recurrence in prostate cancer. Clin Cancer Res. 2003;9:4792–801.

3. Hayward SW, Wang Y, Cao M, Hom YK, Zhang B, Grossfeld GD, et al. Malignant transformation in a nontumorigenic human prostatic epithelial cell line. Cancer Res. 2001;61:8135–42.

4. Olumi AF, Grossfeld GD, Hayward SW, Carroll PR, Tlsty TD, Cunha GR. Carcinoma-associated fibroblasts direct tumor progression of initiated human prostatic epithelium. Cancer Res. 1999;59:5002–11.

5. Gleave M, Hsieh JT, Gao CA, von Eschenbach AC, Chung LW. Acceleration of human prostate cancer growth in vivo by factors produced by prostate and bone fibroblasts. Cancer Res. 1991;51:3753–61.

6. Placencio VR, Sharif-Afshar AR, Li X, Huang H, Uwamariya C, Neilson EG, et al. Stromal transforming growth factor-beta signaling mediates prostatic response to androgen ablation by paracrine Wnt activity. Cancer Res. 2008;68:4709–18.

7. Qi J, Tripathi M, Mishra R, Sahgal N, Fazli L, Ettinger S, et al. The E3 ubiquitin ligase Siah2 contributes to castration-resistant prostate cancer by regulation of androgen receptor transcriptional activity. Cancer Cell. 2013;23:332–46.

8. De Sousa EMF, Vermeulen L, Fessler E, Medema JP. Cancer heterogeneity—a multifaceted view. EMBO Rep. 2013;14:686–95.

9. Kiskowski MA, Jackson RS 2nd, Banerjee J, Li X, Kang M, et al. Role for stromal heterogeneity in prostate tumorigenesis. Cancer Res. 2011;71:3459–70.

10. Bhowmick NA, Ghiassi M, Aakre M, Brown K, Singh V, Moses HL. TGF-beta-induced RhoA and p160ROCK activation is involved in the inhibition of Cdc25A with resultant cell-cycle arrest. Proc Natl Acad Sci USA. 2003;100:15548–53.

11. Brennen WN, Chen S, Denmeade SR, Isaacs JT. Quantification of mesenchymal stem cells (MSCs) at sites of human prostate cancer. Oncotarget. 2013;4:106–17.

12. Fuyuhiro Y, Yashiro M, Noda S, Kashiwagi S, Matsuoka J, Doi Y, et al. Upregulation of cancer-associated myofibroblasts by TGF-beta from scirrhous gastric carcinoma cells. Br J Cancer. 2011;105:996–1001.

13. Fonsatti E, Altomonte M, Nicotra MR, Natali PG, Maio M. Endoglin (CD105): a powerful therapeutic target on tumor-associated angiogenetic blood vessels. Oncogene. 2003;22:6557–63.

14. Beer TM, Armstrong AJ, Rathkopf DE, Loriot Y, Sternberg CN, Higano CS, et al. Enzalutamide in metastatic prostate cancer before chemotherapy. N Engl J Med. 2014;371:424–33.

15. Beltran H, Tagawa ST, Park K, MacDonald T, Milowsky MI, Mosquera JM. et al. Challenges in recognizing treatment-related neuroendocrine prostate cancer. J Clin Oncol. 2012;30:e386–89.

16. Aggarwal RR, Feng FY, Small EJ. Emerging categories of disease in advanced prostate cancer and their therapeutic implications. Oncology. 2017;31:467–74.

17. Dayyani F, Varkaris A, Araujo JC, Song JH, Chatterji T, Trudel GC, et al. Increased serum insulin-like growth factor-1 levels are associated with prolonged response to dasatinib-based regimens in metastatic prostate cancer. Prostate. 2013;73:979–85.

18. Banerjee J, Mishra R, Li X, Jackson RS 2nd, Sharma A, et al. A reciprocal role of prostate cancer on stromal DNA damage. Oncogene. 2014;33:4924–31.

19. True LD, Zhang H, Ye M, Huang CY, Nelson PS, von Haller PD, et al. CD90/THY1 is overexpressed in prostate cancer-associated fibroblasts and could serve as a cancer biomarker. Mod Pathol. 2010;23:1346–56.

20. Zhao H, Peehl DM. Tumor-promoting phenotype of CD90hi prostate cancer-associated fibroblasts. Prostate. 2009;69:991–1000.

21. R2: Genomics Analysis and Visualization Platform (http://r2.amc.nl).

22. Erho N, Crisan A, Vergara IA, Mitra AP, Ghadessi M, Buerki C, et al. Discovery and validation of a prostate cancer genomic classifier that predicts early metastasis following radical prostatectomy. PLoS ONE. 2013;8:e66855.

23. Beltran H, Rickman DS, Park K, Chae SS, Sboner A, MacDonald TY, et al. Molecular characterization of neuroendocrine prostate cancer and identification of new drug targets. Cancer Discov. 2011;1:487–95.

24. Li X, Placencio V, Iturregui JM, Uwamariya C, Sharif-Afshar AR, Koyama T, et al. Prostate tumor progression is mediated by a paracrine TGF-beta/Wnt3a signaling axis. Oncogene. 2008;27:7118–30.

25. Nolan-Stevaux O, Zhong W, Culp S, Shaffer K, Hoover J, Wickramasinghe D, et al. Endoglin requirement for BMP9 signaling in endothelial cells reveals new mechanism of action for selective anti-endoglin antibodies. PLoS ONE. 2012;7:e50920.

26. Zhu Y, Xu Y, Helseth DL Jr., Gulukota K, Yang S, Pesce LL, et al. Zodiac: a comprehensive depiction of genetic interactions in cancer by integrating TCGA data. J Natl Cancer Inst. 2015;107:djv129.

27. Kanayama M, Hayano T, Koebis M, Maeda T, Tabe Y, Horie S, et al. Hyperactive mTOR induces neuroendocrine differentiation in prostate cancer cell with concurrent up-regulation of IRF1. Prostate. 2017;77:1489–98.

28. Sun F, Zhang ZW, Tan EM, Lim ZLR, Li Y, Wang XC, et al. Icaritin suppresses development of neuroendocrine differentiation of prostate cancer through inhibition of IL-6/STAT3 and Aurora kinase A pathways in TRAMP mice. Carcinogenesis. 2016;37:701–11.

29. Romero D, O'Neill C, Terzic A, Contois L, Young K, Conley BA, et al. Endoglin regulates cancer-stromal cell interactions in prostate tumors. Cancer Res. 2011;71:3482–93.

30. Ghajar CM, Peinado H, Mori H, Matei IR, Evason KJ, Brazier H, et al. The perivascular niche regulates breast tumour dormancy. Nat Cell Biol. 2013;15:807–17.

31. Bussard KM, Mutkus L, Stumpf K, Gomez-Manzano C, Marini FC. Tumor-associated stromal cells as key contributors to the tumor microenvironment. Breast Cancer Res. 2016;18:84.

32. Wadosky KM, Koochekpour S. Molecular mechanisms underlying resistance to androgen deprivation therapy in prostate cancer. Oncotarget. 2016;7:64447–70.

33. Mu P, Zhang Z, Benelli M, Karthaus WR, Hoover E, Chen CC, et al. SOX2 promotes lineage plasticity and antiandrogen resistance in TP53- and RB1-deficient prostate cancer. Science. 2017;355:84–88.

34. Joesting MS, Cheever TR, Volzing KG, Yamaguchi TP, Wolf V, Naf D, et al. Secreted frizzled related protein 1 is a paracrine modulator of epithelial branching morphogenesis, proliferation, and secretory gene expression in the prostate. Dev Biol. 2008;317:161–73.

35. Zheng L, Sun D, Fan W, Zhang Z, Li Q, Jiang T. Diagnostic value of SFRP1 as a favorable predictive and prognostic biomarker in patients with prostate cancer. PLoS ONE. 2015;10:e0118276.

36. Esteve P, Sandonis A, Ibanez C, Shimono A, Guerrero I, Bovolenta P. Secreted frizzled-related proteins are required for Wnt/

37. Siamakpour-Reihani S, Caster J, Bandhu Nepal D, Courtwright A, Hilliard E, Usary J, et al. The role of calcineurin/NFAT in SFRP2 induced angiogenesis—a rationale for breast cancer treatment with the calcineurin inhibitor tacrolimus. PLoS ONE. 2011;6:e20412.

38. Sun Y, Zhu D, Chen F, Qian M, Wei H, Chen W, et al. SFRP2 augments WNT16B signaling to promote therapeutic resistance in the damaged tumor microenvironment. Oncogene. 2016;35:4321–34.

39. Bovolenta P, Esteve P, Ruiz JM, Cisneros E, Lopez-Rios J. Beyond Wnt inhibition: new functions of secreted Frizzled-related proteins in development and disease. J Cell Sci. 2008;121:737–46.

40. Kawano Y, Diez S, Uysal-Onganer P, Darrington RS, Waxman J, Kypta RM. Secreted Frizzled-related protein-1 is a negative regulator of androgen receptor activity in prostate cancer. Br J Cancer. 2009;100:1165–74.

41. Joesting MS, Perrin S, Elenbaas B, Fawell SE, Rubin JS, Franco OE, et al. Identification of SFRP1 as a candidate mediator of stromal-to-epithelial signaling in prostate cancer. Cancer Res. 2005;65:10423–30.

42. Miyata Y, Mitsunari K, Asai A, Takehara K, Mochizuki Y, Sakai H. Pathological significance and prognostic role of microvessel density, evaluated using CD31, CD34, and CD105 in prostate cancer patients after radical prostatectomy with neoadjuvant therapy. Prostate. 2015;75:84–91.

43. Degraff DJ, Aguiar AA, Sikes RA. Disease evidence for IGFBP-2 as a key player in prostate cancer progression and development of osteosclerotic lesions. Am J Transl Res. 2009;1:115–30.

44. Laskaratos FM, Rombouts K, Caplin M, Toumpanakis C, Thirlwell C, Mandair D. Neuroendocrine tumors and fibrosis: an unsolved mystery? Cancer. 2017;123:4770–90.

45. Zikusoka MN, Kidd M, Eick G, Latich I, Modlin IM. The molecular genetics of gastroenteropancreatic neuroendocrine tumors. Cancer. 2005;104:2292–309.

46. Igarashi A, Fukagai T, Morita M, Hayashi K, Koshikiya A, Ogawa Y, et al. Initial experience of the enzalutamide treatment for castration-resistant prostate cancer. Nihon Hinyokika Gakkai Zasshi. 2016;107:155–61.

47. Karzai FH, Apolo AB, Cao L, Madan RA, Adelberg DE, Parnes H, et al. A phase I study of TRC105 anti-endoglin (CD105) antibody in metastatic castration-resistant prostate cancer. BJU Int. 2015;116:546–55.

48. Franco OE, Jiang M, Strand DW, Peacock J, Fernandez S, Jackson RS 2nd, et al. Altered TGF-beta signaling in a subpopulation of human stromal cells promotes prostatic carcinogenesis. Cancer Res. 2011;71:1272–81.

49. Stark HJ, Baur M, Breitkreutz D, Mirancea N, Fusenig NE. Organotypic keratinocyte cocultures in defined medium with regular epidermal morphogenesis and differentiation. J Invest Dermatol. 1999;112:681–91.

50. Gao J, Aksoy BA, Dogrusoz U, Dresdner G, Gross B, Sumer SO et al.Integrative analysis of complex cancer genomics and clinical profiles using the cBioPortal. Sci Signal. 2013; 6:pl1.

51. Cerami E, Gao J, Dogrusoz U, Gross BE, Sumer SO, Aksoy BA. et al.The cBio cancer genomics portal: an open platform for exploring multidimensional cancer genomics data.Cancer Discov. 2012;2:401–04.